International Journal of Signal Processing, Image Processing and Pattern Recognition
Vol.9, No.1 (2016), pp.347-360
http://dx.doi.org/10.14257/ijsip.2016.9.1.33

Multi-Focus Image Fusion using Self-Similarity and Depth Information in Nonsubsampled Shearlet Transform Domain

Liu Shuaiqi[a,b], Zhu Zhihui[c], Li Huiya[a,b,*], Zhao Jie[a,b] and Wen Xin[a,b]

a Hebei University, College of Electronic and Information Engineering, Baoding, China, 071000
b Key Laboratory of Digital Medical Engineering of Hebei Province, Baoding, China, 071000
c Colorado School of Mines, Department of Electrical Engineering and Computer Science, Colorado, USA, 80401
E-mail: shdkj-1918@163.com,zzhu@mines.edu,2241421490@qq.com

Abstract

Combined with the shared similarity among multiple source images and depth of field in a camera, a new image fusion algorithm based on nonsubsampled shearlet transform (NSST) domain is proposed. First, NSST is utilized for decomposition of the source images, the low frequency coefficients is fused by weight votes in the structure-driven regions by using shared similarity and depth of field (SSSID), and then apply larger sum-modified-Laplacian (SML) with depth of field to the high frequency coefficients, finally the fusion image is gained after we do the inverse NSST to the fused coefficients. The algorithm can not only preserve the information of the source images well, but also suppress pixel distortion due to nonlinear operations in transform domain. Experimental results demonstrate that the proposed method outperforms the state-of-the-art transform domain fusion methods on image quality and objective fusion criteria.

Keywords: *image fusion, nonsubsampled shearlet transform, self-similarity, depth information*

1. Introduction

Image fusion technique aims at generating a clear and acceptable to human vision panoramic image by fusing comprehensive and redundant information from a set of source images of the same scene [1]. The source images can not reflect the panoramic scene from limited focal length of the camera. So fused image will be more suitable for machine processing and human perception than any individual source image [2]. Generally, multi-focus image fusion can be divided into three levels: pixel level fusion, feature level fusion and decision level fusion [3], and in our paper, we focuses on pixel-level fusion technique. Image fusion method at pixel-level can be divided into two categories: spatial domain algorithms and transform domain algorithms. The spatial domain algorithms mainly include principal component analysis [4, 5], guided filtering based method [6] and so on. The transform domain algorithms are mainly based on multiresolution geometric analysis (MGA) tool domain, such as image fusion algorithm based on wavelet [7, 8], ripplet [9], contourlet [10-12], shearlet [13, 14], surfacelet [15], trained dictionaries [16, 17].

In order to obtain a good image fusion effect, fusion algorithm needs to satisfy three characteristics. Firstly, fused image requires retaining the most information of the source images. Secondly, artificial textures should not be introduced to fused image, which means that fused image should have spatial smoothness. Finally, fusion algorithm should

* Corresponding Author

ISSN: 2005-4254 IJSIP

have robustness so that it can be applied to image fusion between different source images. MGA tools mainly contain discrete wavelet transform (DWT), contourlet transform, non-subsampled contourlet transform (NSCT) [12] and shearlet transform (ST) [14]. They are all successfully applied to image fusion. Contourlet transform is computationally simple and can represent images sparsely, it has been widely applied to image fusion algorithms, such as in [10-12, 19]. However, using contourlet transform for image decomposition will generate frequency aliasing and translational variability [19]. Then non-subsampled Laplacian transform and non-subsampled directional filter to construct NSCT. Though NSCT-based image fusion method arrive satisfactory fusion performance, the high computational complexity cause it is difficult to be applied to real time applications. Different to NSCT, ST [20-23] has a similar mathematical framework to DWT. The shearing filters in ST has smaller support sizes than directional filter in contourlet, so shear filters can help accelerate the computation speed of ST [23-25]. However, ST lack shift-variance and this will lead some artifacts when fused by using ST. In order to overcome the disadvantages of NSCT an ST, in [20], the author gives the construction of NSST by combining nonsubsampled laplacian transform with shearing filters. Compared with current MGA tools, NSST is not only shift-invariance, but also can have better sparse representation ability and much faster computational speed. So, more research should be doing in the field of image fusion based on NSST.

Although many transform domain algorithms methods produce nice images, they lead to pixel distortion due to nonlinear operations in the transform domain [18]. On the contrary, much less distortions are introduced if linear fusion rules in the spatial domain, e.g. the maximum rule, directly choose the pixel values in a well-focused region [18]. But the shape of a region will seriously affect fused images. For example, the commonly used isotropic square regions in the spatial domain will easily lead to blocky artifacts in blurred areas around the edge [18]. Guo D, *et. al.*, proposed structure-driven regions by using the self-similarity of a single image and the shared similarity among multiple source images in [18]. And they also proposed a new method which can refine the image clarity by automatically estimating depth information of blurred images.

Considering the advantages of MGA tools and SSSID, we can easily get the conclusion as follows. First, NSST has significant superiorities than other MGA tools and NSST can also be applied to more research fields. Second, SSSID can effectively use two unique characteristics of multi-focus images to enhance the MGA fusion method's spatial continuity. As a result, we attempt to combine the advantages of both NSST and SSSID together, and proposes a novel multi-focus image fusion method based on NSST and SSSID.

This paper is organized as follows. In Section 2, we give a brief review of NSST theory. In Section 3, we introduce the working principle of SSSID. In Section 4, we give the steps of the new image fusion algorithm based on NSST and SSSID. In Section 5, we demonstrate the experimental results of the proposed and the comparisons with other typical transform domain fusion methods. And in the last section, we explore some conclusions.

2. Non-Subsampled Shearlet Transform

Shearlet transform is a new multi-scale geometric analysis algorithm which inherits advantages of contourlet and curvelet transform [23]. Shearlet transform theory is based on composite wavelets. In dimension $n = 2$, the affine systems with composite dilations are the collections of the form [20, 21]:

$$\Omega_{AB}(\psi) = \left\{ \begin{array}{l} \psi_{j,l,k}(\boldsymbol{x}) = \left|\det \mathbf{A}\right|^{j/2} \psi\left(\mathbf{B}^{l}\mathbf{A}^{j}\boldsymbol{x} - \boldsymbol{k}\right) \\ : j,l \in Z, \boldsymbol{k} \in Z^{2} \end{array} \right\} \tag{1}$$

where $\psi \in L^2(R^2), \boldsymbol{A}, \boldsymbol{B}$ are 2×2 invertible matrices and $|\det \boldsymbol{B}| = 1$.

When for any $f \in R^2$, $\Omega_{\boldsymbol{AB}}(\psi)$ forms a Parseval frames(also called tight frame), we call the elements of $\Omega_{\boldsymbol{AB}}(\psi)$ composite Wavelet. And the dilations $\boldsymbol{A}^j$ are associated with scale transformations, while the matrices $\boldsymbol{B}^l$ are associated to area-preserving geometrical transform, such as rotations and shear [20-22]. We consider a special example of composite wavelets in $L^2(R^2)$ called shearlet. That is let $\boldsymbol{A} = \boldsymbol{A}_0 = \begin{pmatrix} 4 & 0 \\ 0 & 2 \end{pmatrix}$ is the anisotropic dilation matrix, and $\boldsymbol{B} = \boldsymbol{B}_0 = \begin{pmatrix} 1 & 1 \\ 0 & 1 \end{pmatrix}$ is shear matrix in form (1), then ,we can construct a tiling of the frequency like Figure 1.

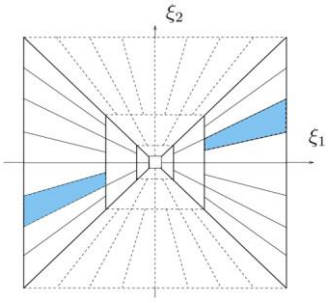

Figure 1. The Tiling of the Frequency Plane Induced by the Shearlet

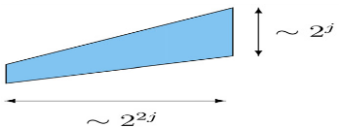

Figure 2. The Frequency Support of Shearlet

Let $\psi_{j,l,k}^{(\theta)}(\boldsymbol{x}) = 2^{\frac{3j}{2}} \psi^{(\theta)}\left(\mathbf{B}_1^l \mathbf{A}_1^j \boldsymbol{x} - k\right)$, That is, each element $\hat{\psi}_{j,l,k}$ is supported on a pair of trapezoids, of approximate size $2^{2j} \times 2^j$, oriented along lines of slope $l2^{-j}$, see Figure 2.

If $f \in L^2\left(R^2\right)$, then its continuous shearlet transform is defined as:

$$SH_\psi = \left\langle f, \psi_{j,l,k}^{(\theta)} \right\rangle \tag{2}$$

where $j \geq 0, l = -2^j, 2^j - 1, k \in \square^2, \theta = 0,1$.

The discretization process of NSST [21] is composed of two phases: multi-scale factorization and multi-orientation factorization. Non-subsampled pyramid is utilized to complete multi-scale factorization, which can produce $(k+1)$ sub-images which consist of one low frequency image and k high frequency images whose sizes are all the same as the source image, where k denotes the number of decomposition levels. The multi-orientation factorization in NSST is realized via improved shearing filters. The shearing filter used in standard shearlet is implemented by the translation operation of the window function in pseudo-polar coordinate system, which includes a down-sampling operation. So it is not shift-invariant. NSST makes the standard shearing filter map from pseudo-polar coordinate systems into Cartesian system to satisfy the property of shift-invariance

[21]. Applying NSST in image fusion can not only reduce the edge blur, but also preserve more useful information for the fusion image.

3. Shared Similarity Regions and Depth Information

In [18], the authors proposed adaptive fusion regions by using image similarity information. They also utilized the depth information to refine spatial continuity. In this section, we give reviews about these contexts.

First, we give the definition of shared similarity regions. The adaptive region is generated using the shared similarity of source images. Images are first divided into multiple overlapped square patches, and similar patches are searched [18, 26]. In [18], a shared self-similarity of source images is defined as follows to generate an adaptive region of pixels for fusion. Given a reference patch $P_r \in R^{m\times m}$ and a region $W(r) \in R^{m\times m}$ centered at pixel r, the similarity of any candidate patch $P_q \in R^{m\times m}$ to the P_r is defined as

$$\eta_q = \left\| P_q - P_r \right\|_F \tag{3}$$

where $\left\| A_M \right\|_F = \sqrt{\sum_{i=1}^{I}\sum_{j=1}^{J}\left|a_{ij}\right|}$ denotes the Frobenius norm of matrix $A_M = (a_{ij})$. By sorting the η_q by the descending order for all the patches in this region, the most k similar patches to P_r are found and the collection of this patches are expressed as $L_W(r) = \left\{P_{q_1}, P_{q_2}, ..., P_{q_k}\right\}$. Similar patches shared by both $L_{W^A}(r)$ and $L_{W^B}(r)$ are

$$L_W^S(r) = L_{W^A}(r) \bigcap L_{W^B}(r) \tag{4}$$

where $L_W^S(r)$ is one of adaptive regions for fusion, $W^A(r)$ and $W^B(r)$ denote the same region of source images f^A and f^B, respectively. The locations and the number of similar patches of each adaptive region vary with the shared similarity of source images. For example, the adaptive region is composed of 4 similar patches as shown in Figure 3.

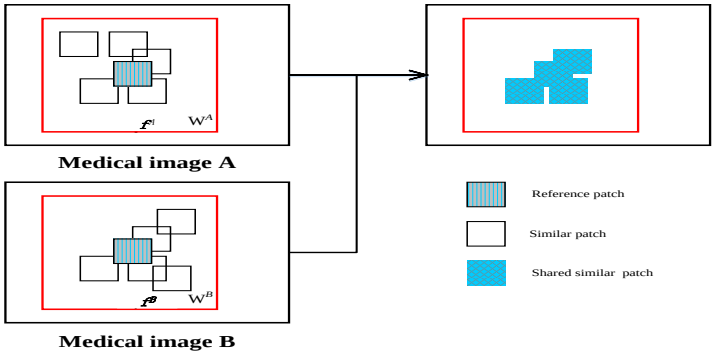

Figure 3. An Adaptive Region of Shared Similar Patches

Then, depth information to refine spatial continuity is introduced in [18]. $d(r)$ denotes the distance between the focal plane and the object whose location corresponds to the image pixel r. When an object is placed at the focal plane, all the rays from a point of the object will converge to a single sensor point and the image will appear sharp. Rays from a point of another object at $d(r)$ will reach multiple sensor points and result in a blurred

image. Let $s(r)$ denote the diameter of the circle of confusion. In [27], a defocus map estimation method is automatically estimating by the assumption of the linear response camera $d(r)\alpha s(r)$. The whole estimation process is shown in [18, 27]. In the follow of our paper, we will use the same fusion rules method as in [18] to fuse the low-frequency coefficients of NSST, and use larger SML which refining by the depth information to fuse the high-frequency coefficients of NSST.

4. Image Fusion based on SSSID

This paper utilizes NSST which is translational invariant to decompose images. The transform suppresses the pseudo Gibbs effect well without increasing computational complexity. The low-frequency coefficients reserve the main spatial information of the source images, so we can directly use SSSID to get the fused image. The sum-modified-Laplacian (SML) proposed in [6] is a better representation of the regional energy function of the image edge details, and has a good effect in selecting the high-frequency coefficients. Therefore, this paper utilizes depth information to smooth the high-frequency coefficients selection map to smooth the spatial continuity of fused image. The proposed image fusion algorithm is described as follows. Without losing of generality, we suppose that A and B are two images with different focuses to fuse, F is fused image. Obviously it is easy to promote it into multiple image fusion.

First, we utilize NSST to decompose image A and B, with decomposition coefficients $C_A^{l,\theta}(r)$ and $C_B^{l,\theta}(r)$. Generally, the coefficients of NSST are $C^{l,\theta}(r)$, where l and θ denote the scale and direction of decomposition respectively. When l is zero, they denote low frequency coefficients, and otherwise they denote high frequency coefficients. r denotes the position of pixel, so the SML at the pixel r is defined as follows [6]:

$$SML^{l,\theta}(r) = \sum_{i \in W(r)} \left[ML^{l,\theta}(i) \right]^2 \tag{5}$$

Let $i = (x, y)$, then:

$$\begin{aligned} ML^{l,d}(x,y) = & |2C^{l,\theta}(x,y) - C^{l,\theta}(x-step,y) - C^{l,\theta}(x+step,y)| \\ & + |2C^{l,\theta}(x,y) - C^{l,\theta}(x,y-step) - C^{l,\theta}(x,y+step)| \end{aligned} \tag{6}$$

where *step* denotes a variable spacing between pixels. Generally, *step* equals to 1.

Thus, the depth information of original sources images can be used as a refinement for the clarity metric on low-frequency coefficients of NSST.

$$CM(r) = SML^{l,\theta}(r) \times \left[d(r) \right]^{-2} \tag{7}$$

The same as [18], CM denotes the clarity metric and f_{Low}^F is the fused image of low-frequency coefficients, and clarity is measured in each adaptive region. If the clarity in an adaptive region $L_W^S(r)$ of f_{Low}^A is larger than f_{Low}^B, one vote will be assigned to all the pixels $j \in L_W^S(r)$ in this adaptive region of f_{Low}^A, meaning

$$v^A(j) = v^A(j) + 1, \; j \in L_W^S(r) \tag{8}$$

where $v^A(j)$ denotes the counter at the spatial location j. The initial values of $v^A(j)$ and $v^B(j)$ are 0 and $v^B(r)$ voting stops until all the adaptive regions are compared. Finally, one can have counter maps $v^A(j)$ and $v^B(j)$ that are in the same size as source images [18]. In the following, $v^A(r)$ and are used to denote the final vote for pixels at location r. At last, use weightings to compose the pixel according to [18].

$$f_{Low}^F(r) = \frac{v^A(r)}{v^A(r)+v^B(r)} f_{Low}^A(r) + \frac{v^B(r)}{v^A(r)+v^B(r)} f_{Low}^B(r) \tag{9}$$

Then, for the high frequency decomposition coefficients $C_A^{l,\theta}(r)$ and $C_B^{l,\theta}(r)$ (l is greater than zero), we apply larger SML with depth information of the source images fusion rule to fuse them. f_{High}^F is the fused image of high-frequency coefficients. And CMD denotes the clarity metric of high-frequency coefficients.

$$CMD(r) = SML^{l,\theta}(r) \times e^{-\frac{[d(r)]^2}{2}} \tag{10}$$

$$f_{High}^F(r) = \begin{cases} f_{High}^A(r) & CMD^A(r) > CMD^B(r) \\ f_{High}^B(r) & CMD^A(r) \le CMD^B(r) \end{cases} \tag{11}$$

Finally, the fused low frequency coefficients f_{Low}^F and the fused high frequency coefficients f_{High}^F are utilized for reconstructing the fused image F through inverse NSST. In conclusion, the framework of the proposed fusion algorithm is shown in Figure 4.

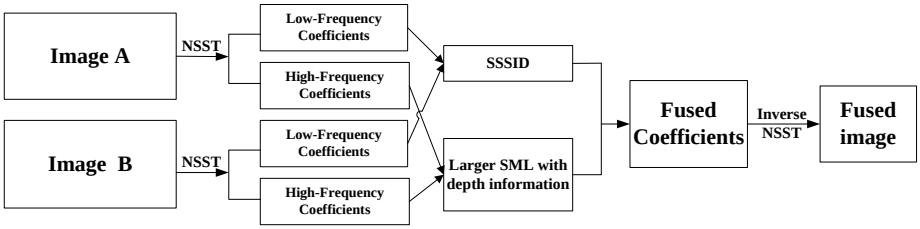

Fig 4. Framework of Image Fusion Algorithm based on NSST-SSSID

5. Experimental Results

We analyze the comparison of our algorithm with other algorithms. In order to evaluate the performance of the proposed fusion method, we use common fusion test images to test it in terms of visual appearance and objective criteria. Fusion method based on MGA tools such as multifocus image fusion method of ripplet transform based on cycle spinning [9], the fusion is also performed using the fusion method of choosing larger SML based on contourlet domain proposed in [11], the fusion method based on the combination of NSCT and PCNN proposed in [12], the adaptive fusion algorithm based on shearlet transform proposed in [13], the fusion method based on the combination of shearlet transform and PCNN proposed in [14] are the comparison methods. $Q^{AB/F}$ metric [11], mutual information (MI) [11] and spatial frequency (SF) [9] are employed as objective criteria. $Q^{AB/F}$ measures the amount of edge information transferred from the source images to the fused images, MI essentially computes how much information from source images is transferred to the fused image, and SF measures the overall activity of

image spatial domain, which can reflect the ability of image expression on tiny details contrast. The larger three index values and the clearer fused image we get, the better fusion performance a method has. In the experiment, default parameters in the shared source codes are used.

First, let us conduct image fusion test on multi-focus images. Fig 5(a) and 5(b) are images of clock with focus on the right and on the left in typical multi-focus images for image fusion test. The size of these two images is 512×512. We utilize the methods proposed in [9, 11-13, 14] and the proposed to fuse respectively. The fused images and difference images (fused images minus the source image) are shown in Figure 5(c)-(t).

(a) source image(focus on the right)

(b) source image(focus on the left)

(c) fused image using method proposed in [9]

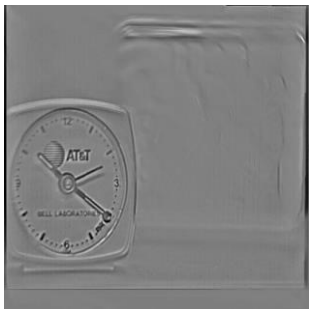

(d) fused image (c) minus source image (a)

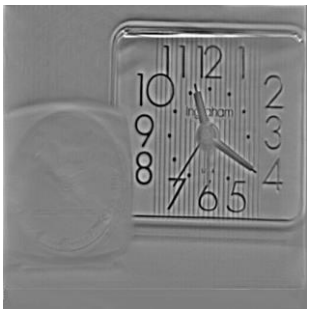

(e) fused image (c) minus source image (b)

(f) fused image using method proposed in [11]

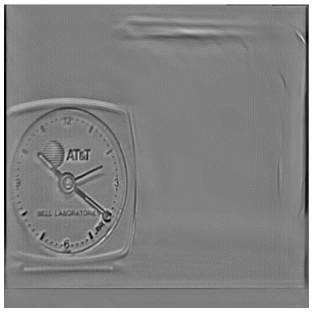

(g) fused image (f) minus source image (a)

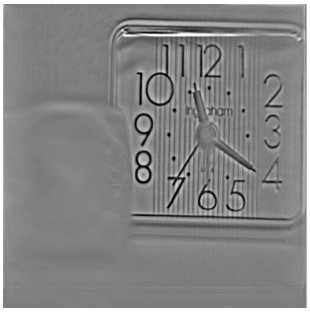

(h) fused image (f) minus source image (b)

(i) fused image using method proposed in [12]

(j) fused image (i) minus source image (a)

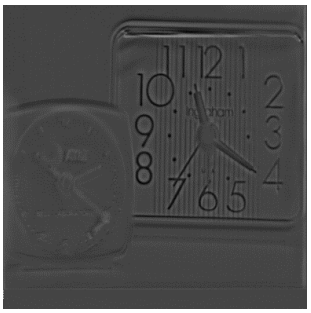

(k) fused image (i) minus source image (b)

(l) fused image using method proposed in [13]

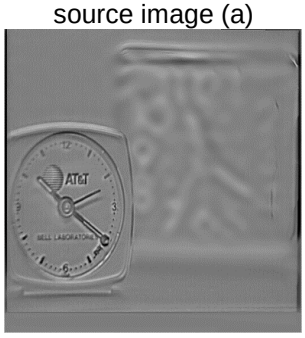

(m) fused image (l) minus source image (a)

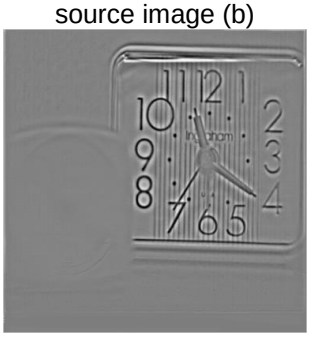

(n) fused image (l) minus source image (b)

(o) fused image using method proposed in [14]

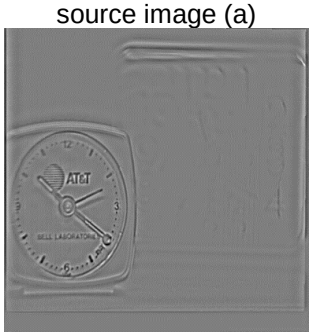

(p) fused image (o) minus source image (a)

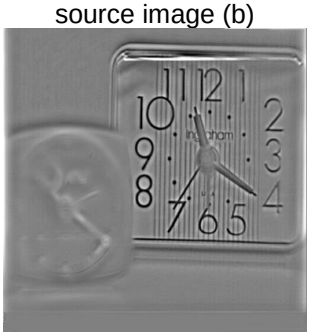

(q) fused image (o) minus source image (b)

(r) fused image using method proposed in this paper

(s) fused image (r) minus source image (a)

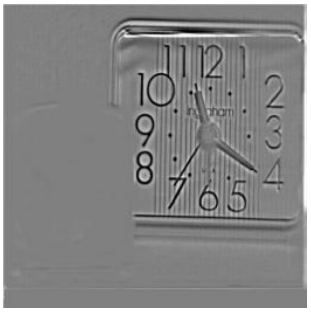

(t) fused image (r) minus source image (b)

Figure 5. Source Images of Clock and Fusion Effects of Each Method

Comparing the top left corner and the area around number 8 of the large clock in fused

image, we can see the proposed method uses image spatial continuity to avoid introducing some artificial texture into the fused image which exists in [9], [11], and [13]. While compared with the algorithm proposed in [14], the proposed method is poorer in these areas, but obviously the gray level is clearer, which can be seen from the difference images. This is mainly because we introduce the NSST to conduct scale decomposition, using its good time-frequency localization characteristic to improve the image gray layering and clarity. Comparing the difference image which the fused image obtained by each method minus Figure 5 (a), we can see the proposed method is better than most other algorithms but it is slightly worse than the algorithm proposed in [12]. However, comparing the difference image obtained by the fused image of the method proposed in [12] misusing Figure 5 (b), the proposed algorithm is much better. Clearly, Figure 5 (t) shows that it does the best in difference image effect. Overall, comparison of the difference image shows that the proposed algorithm has the best visual appearance, the least resulting artificial textures and it also has a significant suppression of artificial textures, which is mainly due to the introduction of spatial continuity by using depth information.

Besides the subjective visual appearance, this paper also uses the six objective criteria mentioned above to investigate the performance of different transform methods. As shown in Table 1, we can see that the proposed algorithm is the highest in the MI, SF and $Q^{AB/F}$ which fully shows that the proposed algorithm does not only consider the information of two differently focused images, but also fully retain the spatial information of both.

Table 1. Objective Criteria using Different Transforms in the Fusion of Figure 4

The fusion methods	$Q^{AB/F}$	MI	SF
The method in [9]	0.6721	6.6882	8.1955
The method in [11]	0.6783	6.7086	8.0840
The method in [12]	0.6775	7.4948	7.9091
The method in [13]	0.6670	6.7204	8.0705
The method in [14]	0.6900	6.7927	8.0202
The proposed method	**0.7020**	**7.9996**	**8.4842**

Then, let us conduct image fusion test on other pair images, Figure 6(a) and 6(b) are flowers images with different focus, Figure 6(c) and 6(d) are disk images with different focus, Figure 6(e) and 6(f) are lab images with different focus, Figure 6(g) and 6(h) are pepsi images with different focus. These images can download from "www.imagefusion.org".

(a) (c) (e) (g)

(b) (d) (f) (h)

Figure 6. Images with different focus, Figure 6. (a, b) , Figure 6. (c, d), Figure 6. (e, f) and Figure 6. (g, h) are flowers, disk, lab and pepsi images with different focus

We utilize the methods proposed in [9, 11-13, 14] and the proposed to fuse respectively. The fused images and difference images which fused images minus the source image are shown in Figure 7(c)-(t).

(a) (g) (m) (s)

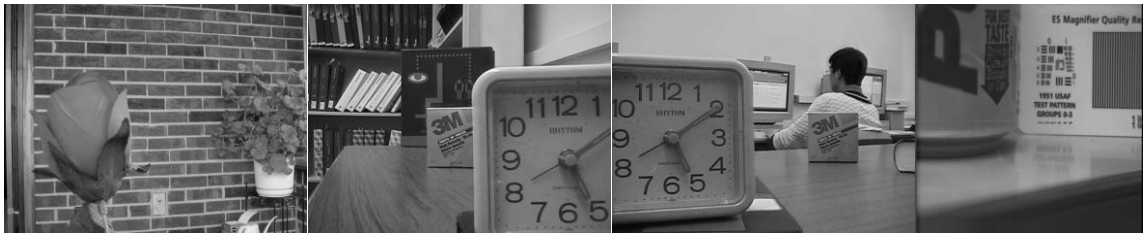

(b) (h) (n) (t)

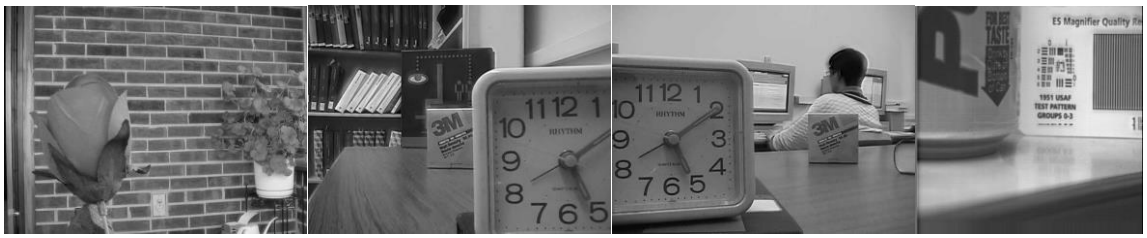

(c) (i) (o) (u)

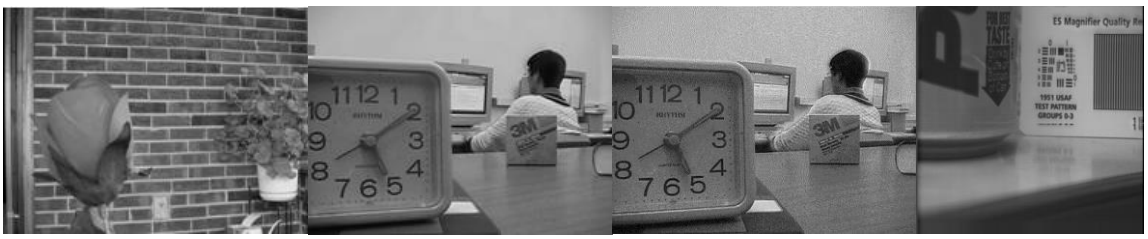

(d) (j) (p) (v)

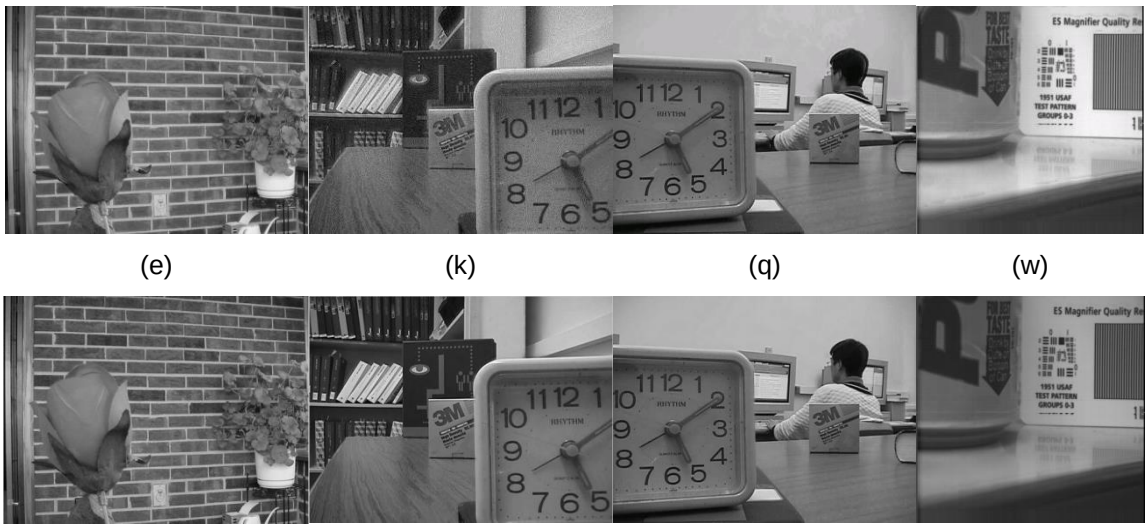

(e) (k) (q) (w)

(f) (l) (r) (x)

Figure 7. The Performance of Each Fusion Method, Figure (a-f), (g-l) , (m-r) and (s-x) Shows the Performance of Each Fusion Method on Flower, disk, lab and pepsi

All the tests in Figure 7 show that the proposed algorithm has the best visual appearance and the least resulting artificial textures, which means that the proposed algorithm has a significant suppression of artificial textures. As well, this paper also uses the objective criteria "MI" and "$Q^{AB/F}$" to investigate the performance of different transform methods. As shown in Figure 8 (a) and (b), from which we can see, the proposed algorithm is the highest in the performance of objective criteria. All the above show that the proposed algorithm is very suitable for fairly complex aerial images of different focus to fuse.

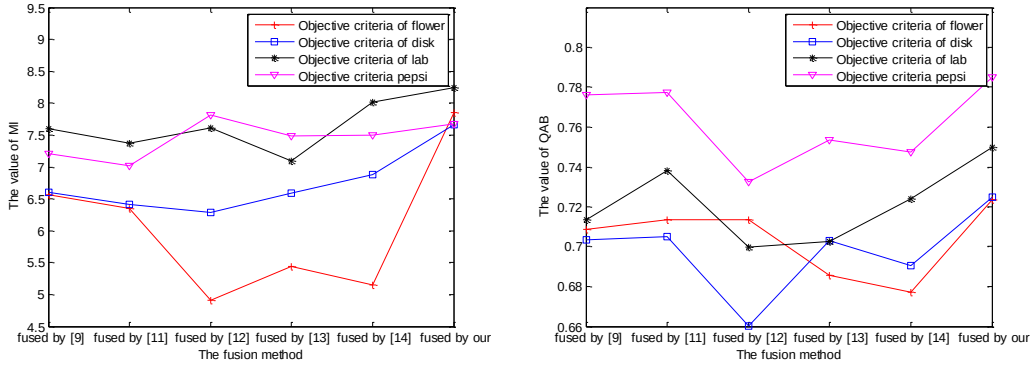

(a) The value of MI (b) The value of Q^{AB}

Figure 8. Objective Criteria using Different Transforms in the Fusion of Figure 7

6. Conclusions

This paper presents an image fusion algorithm based on NSST and SSSID. Based on the traditional image fusion algorithm via frequency domain, the algorithm uses structure-driven regions and depth information to fuse the low-frequency coefficients of NSST. The

depth of source image also is applied to SML of the high frequency coefficients, which can enhance the spatial characteristics in the process of image fusion. Experimental results demonstrate that the proposed method is better than or close to the current popular image fusion algorithms based on MGA tools in terms of both visual appearance and objective criteria. Furthermore, we will apply this method to other image fusion such as medical image fusion.

Acknowledgements

The authors are grateful to Dr. Qu for sharing the SSSID code, Prof. Geng, Miao for sharing the image fusion codes. This work was supported in part by Natural Science Foundation of China under grant 61401308 and 61572063, Natural Science Foundation of Hebei Province under grant 2013210094, Natural Social Foundation of Hebei Province under grant HB15TQ015, Natural Science Foundation of Hebei University under grant 2014-303, Science and technology support project of Baoding City under grant 14ZG036, Open laboratory project of Hebei University under grant sy2015009 and sy2015057, Post-graduate's Innovation Fund Project of Hebei University under grant X2015085.

References

[1] A. Goshtasby, S. Nikolov. Image fusion: advances in the state of the art.Inf. Fusion. 2, 8 (2007).
[2] Y. Liu, Z. Wang. Simultaneous image fusion and denoising with adaptive sparse representation. IET Image Processing. 3, 11 (2014).
[3] W. Huang, Z. Jing. Evaluation of focus measures in multi-focus image fusion. Pattern Recognition Letters. 4, 28 (2007).
[4] Y. H. Jia. Fusion of Landsat TM and SAR images based on principal component analysis. Remote Sensing Technology and Application.1, 13 (1998).
[5] T. Wan, C. C. Zhu, Z. C. Qin. Multifocus image fusion based on robust principal component analysis. Pattern Recognition Letter. 9, 34 (2013).
[6] S. T. Li, X. D. Kang, J. W. Hu. Image fusion with guided filtering. IEEE transactions on Image Processin. 7, 22 (2013).
[7] G. Pajares, J. M. Cruz. A wavelet-based image fusion tutorial. Pattern Recognition. 9, 37 (2004).
[8] Y. Chai, H. Li, Z. Li. Multifocus image fusion scheme using focused region detection and multiresolution. Optics Communications. 19, 284 (2011).
[9] P. Geng, M. Huang, S. Q. Liul. Multifocus image fusion method of Ripplet transform based on cycle spinning. Multimedia Tools and Applications. 1, 11 (2014).
[10] S. Q. Liu, J. Zhao, P. Geng. Medical image fusion based on nonsubsampled direction complex wavelet transform . International Journal of Applied Mathematics and Machine Learning. 1, 1 (2014).
[11] X. B. Qu, J. W. Yan, G. D. Yang. Sum-modified-Laplacian-based multi-focus image fusion method in sharp frequency localized contourlet transform domain. Optics and Processing Engineering,5, 17 (2009)..
[12] X. B. Qu, J. W. Yan, H. Z. Xiao. Image fusion algorithm based on spatial frequency motivated pulse coupled neural networks in nonsubsampled contourlet transform domain. Acta Automatica Sinica. 12, 34 (2008).
[13] Q. G. Miao, C. Shi, P. E. Xu. A novel algorithm of image fusion using shearlets. Optics Communications. 6. 284 (2011).
[14] P. Geng, Z. Wang, Z. Zhangl. Image fusion by pulse couple neural network with shearlet. Optical Engineering. 6, 51(2012).
[15] Q. Zhang, L. Wang, Z.Mal. A novel video fusion framework using surfacelet transform. Optics Communications. 13, 285 (2012).
[16] L. Chen, J. Li, C. L. Chen. Regional multifocus image fusion using sparse representation. Optics express. 4, 21 (2013).
[17] S. B. Gao, Y. M. Cheng, Y. Q. Zhao. Method of visual and infrared fusion for moving object detection. Optics letters. 11, 38 (2013).
[18] D. Guo, J. Yan, X. Qu. High quality multi-focus image fusion using self-similarity and depth information. Optics Communications. 1, 338 (2015).
[19] S. Q. Liu, S. H. Hu, Y. Xiao. SAR image de-noised based on wavelet-contourlet transform with cycle spinning. Signal Processing. 6, 27 (2011).
[20] G. Easley, D. Labate, W. Q. Lim. Sparse directional image representation using the discrete shearlets transform. Applied and Computational Harmonic Analysis. 1, 25 (2008).
[21] G. Kutyniok, J. Lemvig, W. Q. Lim. Compactly supported shearlets are optimally sparse. Journal of Approximation Theory. 11, 163 (2011).

[22] W. Q. Lim. The discrete shearlets transform: A new directional transform and compactly supported shearlets frames. IEEE Trans. Image Proc. 5, 19 (2010).
[23] S. Liu, S. Hu, Y. Xiao. Image separation using wavelet-complex shearlet dictionary. Journal of Systems Engineering and Electronics. 2, 25 (2014).
[24] W. Kong, L. Zhang, Y. Lei. Novel fusion method for visible light and infrared images based on NSST-SF-PCNN. Infrared Physics & Technology. 65 (2014).
[25] S. Q. Liu, S. H. Hu, Y. Xiao. Bayesian shearlet shrinkage for SAR image de-noising via sparse representation. Multidimensional Systems and Signal Processing. 4, 25 (2014).
[26] X. B. Qu, Y. Hou, F. Lam. Magnetic resonance image reconstruction from undersampled measurements using a patch-based nonlocal operator. Medical image analysis. 6, 18 (2014).
[27] S. Zhuo, T. Sim. Defocus map estimation from a single image. Pattern Recognition. 9, 44 (2011).